JOURNAL OF SOLID STATE CHEMISTRY **140,** 20–28 (1998)
ARTICLE NO. SC987811

Reversible Oxidation/Reduction in the $CeTaO_{4+\delta}$ System: a TEM and XRD Study

G. Drew, R. L. Withers[1], A-K. Larsson, and S. Schmid

Research School of Chemistry, Australian National University, Canberra, ACT 0200, Australia

Received December 10, 1997; accepted March 6, 1998

A detailed TEM and XRD study has been made of the basic crystallography (unit cells, space group symmetries, and twin relationships) of each of the three oxidized phases which occur in the $CeTaO_{4+\delta}$ system, their structural relationship to stoichiometric $Ce^{+III}TaO_4$, and their temperature-dependent redox reactions. Such crystallographic knowledge is essential to understand the structural relationships between the various phases and to gain insight into the oxidation/reduction mechanisms allowing the formation of the oxidized phases. Twinning is found to be endemic in stoichiometric $Ce^{+III}TaO_4$ as well as in each of the oxidized Series 2, 3, and 4 phases; the twin plane relating the twin variants is derived in each case. © 1998 Academic Press

1. INTRODUCTION

The effective valence state of cerium, i.e., the ratio of Ce^{+III} to Ce^{+IV} ions, and hence the oxygen content of the compound $CeTaO_{4+\delta}$, is known to be extraordinarily sensitive to temperature as well as to the partial pressure of oxygen in the surrounding atmosphere (1–4). Thus fully reduced $Ce^{+III}TaO_4$ (which can only be obtained at room temperature by preparing it above $\sim$1270°C and rapidly quenching) can be reversibly oxidized and reduced at temperatures between about 300 and 1000°C.

In a comprehensive TGA/XRPD study, Negas *et al.* (1) first discovered the existence of three distinct $CeTaO_{4+\delta}$ solid solution fields, each of which can be prepared by heating stoichiometric $CeTaO_4$ at elevated temperatures for varying lengths of time. The virtually fully oxidized, so-called Series 2 reaction product, $CeTaO_{4+\delta}$ with $0.50 > \delta > 0.48$, was prepared by heating stoichiometric $CeTaO_4$ for several days at temperatures between about 350 and 575°C. Heating between 575 and 900°C for a much shorter time, $\sim$several hours, gave rise to the Series 3 reaction product, $CeTaO_{4+\delta}$ with $0.18 > \delta > 0.09$, while heating between about 900 and 950° C and then cooling gave rise to the Series 4 reaction product, $CeTaO_{4+\delta}$ with $0.40 > \delta > 0.33$. Within each series, δ was found to vary continuously and reversibly as a function of temperature. Rapid transformation from the Series 2 to the Series 3 phase ("... suggesting a transition between structurally similar materials..." (1)) occurs on heating near 600°C and, while sluggish, was reversible on cooling. By contrast, the Series 3-to-Series 4 phase transformation via oxidation on heating was rather sluggish and nonreversible on cooling.

Crystallographic knowledge of these various phases is essential in order to understand the structural relationships between the various phases and to gain insight into the oxidation/reduction mechanisms allowing the formation of the oxygen-rich phases. To date, however, only the crystal structure of stoichiometric $CeTaO_4$ (monoclinic $P2_1/c$, of $LaTaO_4$ type (5)) is known (6). It consists of alternating (100) slabs of corner-connected TaO_6 octahedra (two octahedra wide) separated by (100) slabs of Ce^{+III} ions (see Fig. 1). Santoro *et al.* (6) described the octahedral slabs as being "...perovskite like... with the Ce atoms located in sites similar to the *A* sites of the ABO_3 perovskite structure...". The large rotations of the TaO_6 octahedra apparent in Fig. 1 suggest that a somewhat better analogy would be to the PdF_3 structure type.

From visual inspection of X-ray powder data (2), the Series 3 phase is the most closely related structurally to stoichiometric $CeTaO_4$. Despite problems associated with twinning (2), unit cell dimensions and an apparent space group symmetry have been reported for this Series 3 phase. Unit cell dimensions, but not space group symmetry, have also been reported for the Series 4 phase. Twinning was again a problem and reported as preventing unambiguous symmetry determination (1). Neither unit cell dimensions nor space group symmetry, however, have been reported for the Series 2 phase ("...symmetry and cell parameters... cannot be determined unambiguously... as crystals are twinned or multiple in nature..." (2)). Twinning appears ubiquitous in fully reduced $CeTaO_4$ and in all three oxidized phases (1, 2). Finally, to complicate matters still further, stoichiometric $CeTaO_4$ is known to undergo a further phase transition, a displacive structural phase transition, to a structurally

[1] To whom correspondence should be addressed.

0022-4596/98 $25.00

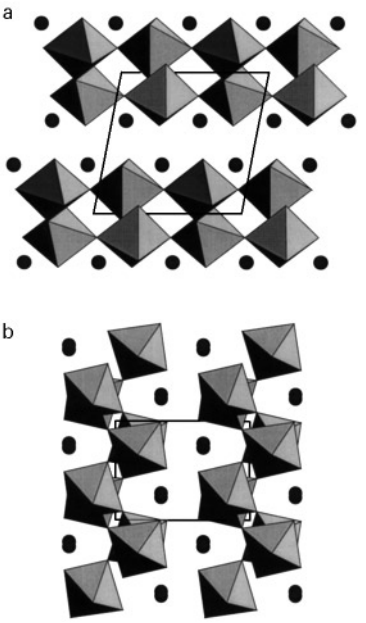

FIG. 1. The crystal structure of stoichiometric $CeTaO_4$ projected along the (a) [100] and (b) [001] directions. The octahedra are TaO_6 octahedra, while the remaining spheres represent Ce^{+III} ions.

closely related orthorhombic phase on heating in vacuo (4, 7)).

The purpose of this paper is to present the results of a combined TEM and powder XRD study of the basic crystallography (unit cells, space groups, and twin relationships) of these various $CeTaO_{4+\delta}$ phases and to explore the structural relationships among them. The advantage of electron diffraction, in the current context, is its ability to reveal weak features of reciprocal space (such as ordering associated with excess oxygen atoms) often missed by powder XRD and to do so from small single crystal regions of real space. The disadvantage, particularly for the current material, is the reducing environment of the TEM column, particularly under an intense electron beam.

2. EXPERIMENTAL

Quantities of the fully reduced $CeTaO_4$ precursor were synthesized from a $2:1 \pm < 0.5\%$ molar ratio of CeO_2 (99.9%, Koch-Light Labs Ltd.) and Ta_2O_5 (99.99%, Aldrich Chem. Co.). The ground and pelleted mixtures were heated at 1000°C for varying times (typically 14 hours) in a platinum vessel, allowed to cool to room temperature, then reground, re-pressed, and heated again (typically for an additional 16 hours) at 1500°C (7). During the second heating stage, the mustard yellow sample changed to a khaki green color. All samples were quenched in water to prevent decomposition to $CeTa_3O_9$ and CeO_2 (1). It was noted that any delay in quenching resulted in the formation of a dark grey phase integrated in the extremities of the pellets, as did the use of acetone as a drying agent. Air quenched specimens were grey throughout.

Representative samples of the Series 2, 3, and 4 oxidized solid solution phases were prepared from portions of the precursor pellets on sheet platinum held in alumina vessels. Heating for 65 hours at 350°C gave rise to the Series 2 phase (a yellow solid that disintegrated on impact with water). Series 3 samples were prepared by heating (typically for three hours) at 650, 750, and 850°C, respectively. The resultant samples were a dark grey color throughout. Series 4 samples were prepared by heating at 925 and 950°C for varying times (1, 3, 7.5, 24, 65, and 165 hours).

Specimens for electron microscopy were prepared by crushing and dispersing onto holey-carbon coated copper grids. These grids were then examined in JEOL 100CX and Philips EM430 transmission electron microscopes (TEMs). XRD data were collected using a Guinier-Hägg camera with Si used as an internal standard.

3. RESULTS AND DISCUSSION

The $CeTaO_4$ Precursor Phase

As expected, the electron diffraction (ED) results confirmed $P2_1/c$ space group symmetry for the stoichiometric $Ce^{+III}TaO_4$ precursor phase. The XRPD refined unit cell dimensions and monoclinic cell angle for this phase, $a = 7.618(3)$, $b = 5.526(2)$, $c = 7.766(4)$ Å, $\beta = 100.96(3)^\circ$, are in good agreement with previously reported results (2, 6).

Twinning made indexation of electron diffraction patterns (EDPs) from this phase (and also from the closely related Series 3 phase—see below) somewhat difficult, in that it was often found that a subset of the Bragg reflections in EDPs taken from opposite ends of an apparent single crystal grain at very nearly the same orientation appeared to superpose more or less exactly and yet the overall EDPs were quite clearly distinct. Fig. 2a, for example, shows a $[2\bar{1}0]_A$ zone axis micro-diffraction pattern taken from one end (the A end) of a particular grain, while Fig. 2b shows the corresponding $[211]_B$ zone axis micro-diffraction pattern taken from the opposite (B end) of the same grain.

Similar A/B pairs of EDPs were obtained at all zone axis orientations found in an $\sim 70^\circ$ tilt series about the c^* reciprocal lattice direction for this particular grain. Fig. 2c, for example, shows the $[1\bar{1}0]_A$ zone axis micro-diffraction pattern taken from the A end of the same grain, while Fig. 2d shows the corresponding $[221]_B$ zone axis micro-diffraction pattern taken from the opposite (B) end of the grain. Any two A/B pairs (such as those shown in Fig. 2) are sufficient to derive an approximate reciprocal space relationship between the two twin orientations. In the present case, this implied reciprocal space relationship is given by $\mathbf{a}_B^* \sim -\mathbf{a}_A^*$, $\mathbf{b}_B^* \sim \mathbf{b}_A^*$, and $2\mathbf{c}_B^* \sim -\mathbf{a}_A^* + 2\mathbf{c}_B^*$. The corresponding real

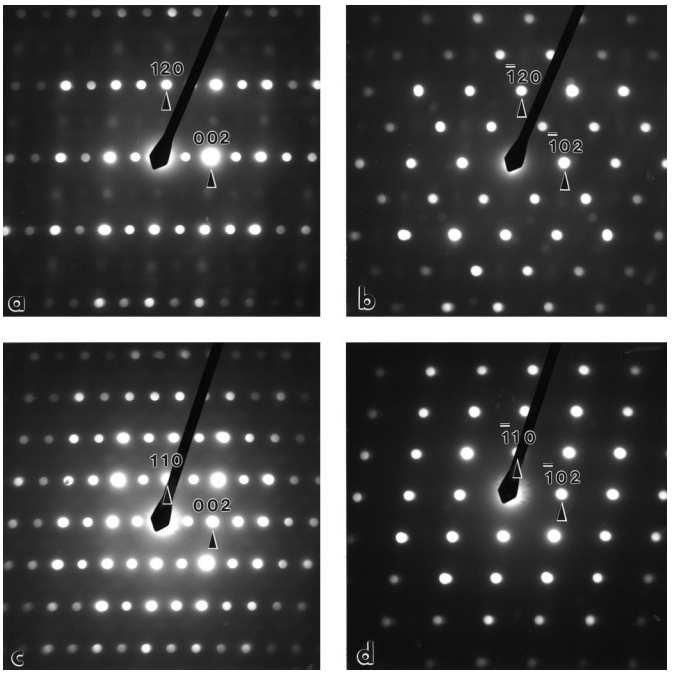

FIG. 2. Twinned A/B pairs of micro-diffraction patterns obtained from stoichiometric $CeTaO_4$ at two distinct zone axis orientations. (a) A $[2\bar{1}0]_A$ zone axis micro-diffraction pattern taken from one end (the A end) of a particular grain. (b) The corresponding $[211]_B$ zone axis microdiffraction pattern taken from the opposite (B end) of the same grain at the same zone axis orientation. (c) The $[1\bar{1}0]_A$ zone axis micro-diffraction pattern taken from the A end of the same grain. (d) The corresponding $[221]_B$ zone axis microdiffraction pattern taken from the opposite (B) end of the grain. Note that a subset of the Bragg reflections in each A/B pair superpose more or less exactly.

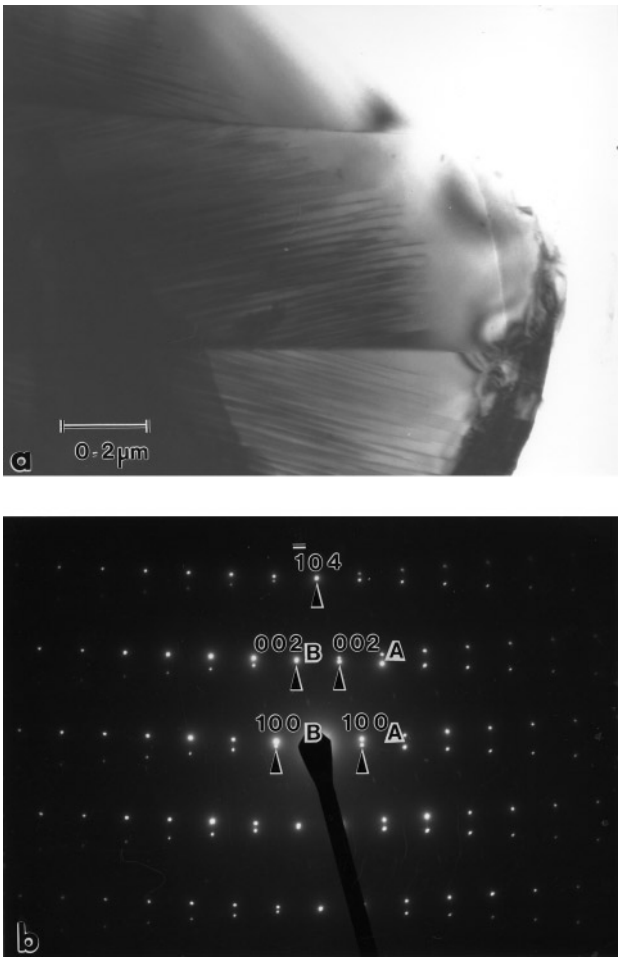

FIG. 3. (a) Bright field image of a typical twin boundary characteristic of both stoichiometric $CeTaO_4$ and the oxidized Series 3 phase. (b) Shows the corresponding [010] zone axis EDP taken from an area that includes both twin orientations. Note that the twinning occurs perpendicular to $4\mathbf{a} + \mathbf{c}$ with a composition plane close to $(\bar{1}04)$.

space relationship is $2\mathbf{a}_B \sim 2\mathbf{a}_A + \mathbf{c}_A$, $\mathbf{b}_B \sim -\mathbf{b}_A$, and $\mathbf{c}_B \sim -\mathbf{c}_A$, respectively.

The exact reciprocal space relationship only becomes apparent from [010] zone axis EDPs taken from areas that include both twin orientations, such as that shown in Fig. 3b. From X-ray precession photographs, Roth *et al.* (2) reported "... twinning which occurs in planes perpendicular to either the **a** or **c** axes or both... ." The only (and very common) type of twinning we have observed, however, is neither perpendicular to **a** nor **c** but rather perpendicular to $4\mathbf{a} + \mathbf{c}$ with a composition plane close to $(\bar{1}04)$ (see Fig. 3a).

The scale of this twinning is typically $\sim 0.5\,\mu m$, which is absolutely characteristic of both the $CeTaO_4$ precursor phase and the closely structurally related Series 3 phase. Indeed, the particular twin boundary and grain shown in Fig. 3a was originally an oxidized Series 3 phase grain. The increase in electron beam intensity required to take the image in Fig. 3a was found to be sufficient to induce a phase transformation to the fully reduced $CeTaO_4$ phase. Such reduction under electron beam irradiation was reasonably common although avoidable provided the electron flux was not excessive. The EDP shown in Fig. 3b was taken after the phase transformation. In this context, the presence of fine scale features running perpendicular to the **c*** directions of both the twin variants is an intriguing observation and may well be related to the mechanism of reduction from the Series 3 phase to the fully reduced $CeTaO_4$ phase.

The crystallography underlying such an apparently unusual high index [401] twin plane is closely related to the existence of a high-temperature monoclinic-to-orthorhombic displacive structural phase transition, which stoichiometric $Ce^{+III}TaO_4$ undergoes when heated in vacuo (at 818°C on heating and 729°C on cooling (4)). While the crystal structure of the orthorhombic high-temperature form has not to date been reported, the crystal structure of isomorphous orthorhombic $LaTaO_4$ has been reported, as has the relationship of the orthorhombic (subscript o/r) cell to the low-temperature monoclinic (subscript m/c) phase (7), i.e., $\mathbf{a}_{o/r} = \frac{1}{2}[4\mathbf{a}_{m/c} + \mathbf{c}_{m/c}]$, $\mathbf{b}_{o/r} = \mathbf{b}_{m/c}$, $\mathbf{c}_{o/r} = \frac{1}{2}\mathbf{c}_{m/c}$ (see Fig. 4).

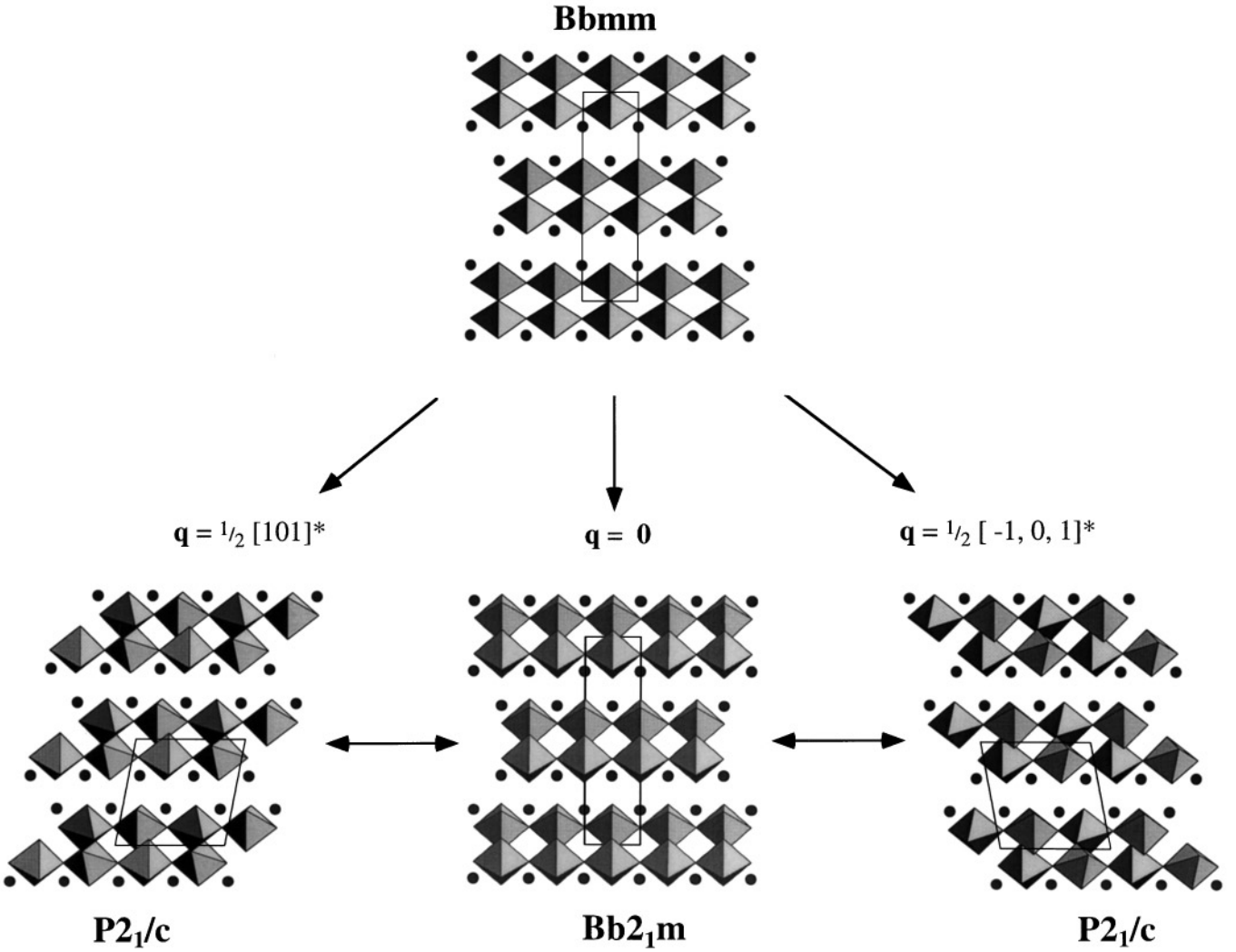

FIG. 4. Shows an $[010]_{o/r} \equiv [010]_{m/c}$ projection (the unit cells are outlined and the c axis horizontal in each case) of a hypothetical *Bbmm* "parent structure" and the orthorhombic and two monoclinic derivative structures which can be obtained therefrom via appropriate displacive modulation. In the case of the orthorhombic $Bb2_1m$ form, this displacive modulation takes the form of a $\mathbf{q} = \mathbf{0}$ displacive mode involving coupled rotation of the TaO_6 octahedra about $[001]_{o/r}$. In the case of the monoclinic $\mathbf{P}2_1/\mathbf{c}$ form, the displacive modulation takes the form of a $\mathbf{q} = \frac{1}{2}\langle 101\rangle^*_{o/r} \equiv \langle 001\rangle^*_{m/c}$ displacive mode involving an ReO_3-to-PdF_3 type rotation (see Fig. 30 of Ref. (8)) about one of two originally symmetry-equivalent $\bar{3}$ axes of the TaO_6 octahedra.

In this latter setting, the high-temperature orthorhombic form has space group symmetry $Bb2_1m$, while the low-temperature monoclinic form has $P2_1/c$ space group symmetry. While $P2_1/c$ is not a subgroup of $Bb2_1m$, both are subgroups of a common *Bbmm* hypothetical "parent structure" (with the same unit cell dimensions as the high-temperature orthorhombic phase) and can be derived therefrom via appropriate displacive modulation (see Fig. 4). In the case of the orthorhombic form, this displacive modulation takes the form of a $\mathbf{q} = \mathbf{0}$ displacive mode involving coupled rotation of the TaO_6 octahedra about $[001]_{o/r}$. In the case of the monoclinic form, the displacive modulation takes the form of a $\mathbf{q} = \frac{1}{2}\langle 101\rangle^*_{o/r} \equiv \langle 001\rangle^*_{m/c}$ displacive mode involving an ReO_3-to-PdF_3 type rotation (see Fig. 30 of Ref. (8)) about one of two originally symmetry-equivalent $\bar{3}$ axes of the TaO_6 octahedra (see Fig. 4). Choice of this $\bar{3}$ axis determines which of the two $P2_1/c$ twin variants shown in Fig. 4 is obtained. Such a picture also explains why the twin plane observed experimentally in the low-temperature monoclinic phase (see Fig. 2b) is, of necessity, $[401]_{m/c} \equiv [200]_{o/r}$.

The Series 3 Phase

Roth *et al.* (2) reported an $a \sim 7.64$, $b \sim 5.50$, $c \sim 3.85$ Å, $\beta \sim 102.7^\circ$ monoclinic unit cell for the $CeTaO_{4+\delta}$, Series 3 solid solution phase with an apparent space group

symmetry of $P2$, Pm or $P2/m$ (2). Electron diffraction investigation of the 650, 750, and 850°C specimens, however, showed that this reported c axis dimension always needed to be doubled to $c \sim 7.70$ Å (see Fig. 5), giving rise to Series 3 substructure reflections (**G**) and unit cell dimensions virtually identical to those of the fully reduced $CeTaO_4$ phase. In addition, however, each of the Series 3 samples was found to show evidence for a weak $\frac{1}{3}\mathbf{b}^*$ modulation, giving rise to additional $\mathbf{G} \pm \frac{1}{3}\mathbf{b}^*$ type satellite reflections (see Fig. 5a), presumably a result of excess oxygen (and Ce^{+III}/Ce^{+IV}) ordering and associated structural relaxation. These additional satellite reflections were sharp for the 650°C specimens, slightly diffuse for the 750°C specimens, and streaked for the 850°C specimens.

Most grains showed the additional modulation. There were, however, significant numbers of grains which did not. The absence of the $\frac{1}{3}\mathbf{b}^*$ modulation in these particular grains is attributed to a transformation to reduced $CeTaO_4$ induced by the reducing conditions of the TEM. As already mentioned, it is quite possible to reduce the oxidized samples in the TEM via excessive electron beam irradiation. It is not possible from EDPs to distinguish the Series 3 phase from the fully reduced $CeTaO_4$ phase on the basis of the subcell reflections alone, except at the [010] zone axis (see Fig. 5b), where the presence of c glide forbidden $h0l$, l odd reflections clearly differentiates the Series 3 phase from the fully reduced $CeTaO_4$ phase (cf. Fig. 5b) with Fig. 3b). A weak first order Laue zone (FOLZ) ring due to the $\frac{1}{3}\mathbf{b}^*$ modulation was always present when zero OLZ (ZOLZ) EDPs such as that shown in Fig. 5b were obtained, confirming that the broken c glide symmetry of the substructure and the $\frac{1}{3}\mathbf{b}^*$ modulation always go together.

XRPD-obtained unit cell dimensions of the Series 3 phase samples were essentially consistent with the temperature-dependent subcell lattice parameters previously reported by Roth *et al.* (2), e.g., $a = 7.616(2)$, $b = 16.459(5) = 3 \times 5.486$, $c = 7.704(2) = 2 \times 3.852$ Å, $\beta = 102.48(2)^\circ$ at 650°C; $a = 7.648(1)$, $b = 16.491(3) = 3 \times 5.497(1)$, $c = 7.712(2) = 2 \times 3.856$ Å, $\beta = 102.67(1)^\circ$ at 750°C, etc. Due to the weak intensity of the $\mathbf{G} \pm \frac{1}{3}\mathbf{b}^*$ type satellite reflections, only a very few such satellite reflections were visible on deliberately overexposed Guinier films—specifically the [121]*, [040]*, and [042]* reflections when indexed with respect to the above cell dimensions.

According to Table I of Roth *et al.* (2), the stoichiometry of the 650°C sample, the sample with sharp $\mathbf{G} \pm \frac{1}{3}\mathbf{b}^*$ type satellite reflections, is close to $CeTaO_{4.17}$. The most likely space group symmetry is $P2_1$. Certainly the c glide perpendicular to **b** of the $CeTaO_4$ phase no longer holds (see Fig. 5b). Nonetheless, the rapidity with which $CeTaO_4$ crystals can be oxidized to the Series 3 phase ("… The crystals change from light green to black during a few hours heating at ~600°C..." (1, 2)) in conjunction with the similarity of the XRD profiles for the Series 3 and $CeTaO_4$ phases suggests that they have a common underlying substructure. The questions of how the excess 0.17 oxygens are arranged in this common ($P2_1/c$) substructure and how the local crystal chemistry adapts to this change remain to be determined. Further work along these lines is in progress.

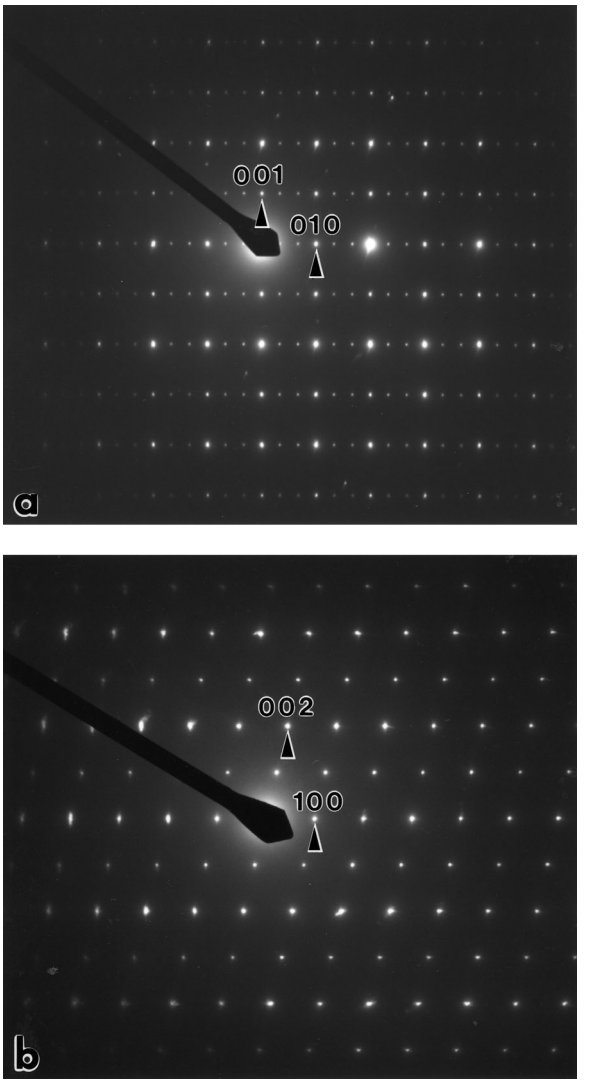

FIG. 5. Shows (a) [100] and (b) [010] zone axis EDPs characteristic of the Series 3, $CeTaO_{4+\delta}$ solid solution phase. Indexation is with respect to an $a \sim 7.6$, $b \sim 5.49$, $c \sim 7.7$ Å, $\beta \sim 102.5^\circ$ sub-cell. Note the existence of additional $\mathbf{G} \pm \frac{1}{3}\mathbf{b}^*$ type satellite reflections in (a) and the presence of $h0l$, l odd, c glide forbidden reflections in (b).

The Series 2 Phase

Neither unit cell dimensions nor space group symmetry have been reported for the Series 2 phase, although Roth *et al.* (2) reported that the "… symmetry may now be triclinic with as yet uninterpreted complications due to

superstructure … " (2). Careful crosscorrelation of electron diffraction and XRD results was required to successfully index the reciprocal lattice of this phase. Triclinic symmetry ($P1$ or $P\bar{1}$) was confirmed with unit cell dimensions and angles given by $a = 7.908(2)$, $b = 6.735(3)$, $c = 12.357(2)$ Å, $\alpha = 80.07(3)^\circ$, $\beta = 77.69(2)^\circ$, and $\gamma = 73.63(3)^\circ$ respectively. The existence of a superstructure (a four times superstructure along the **c*** direction) was also found and is apparent from the [010] and [110] zone axis EDPs shown in Fig. 6.

As for the fully reduced and Series 3 phases, twinning and pseudosymmetry was again endemic. Figure 7a, for example, shows an essentially single twin variant micro-diffraction pattern taken close to a [100] zone axis orientation. Very slight movement of the probe gave rise to the twinned [100] zone axis micro-diffraction pattern shown in Fig. 7b. Such twinning was commonly observed and always occurred perpendicular to the $[01\bar{1}]^*$ direction of reciprocal space. Note that the strong reflections of the two (A and B) twin variants overlap almost exactly in Fig. 7b and define a pseudorectangular reciprocal space sublattice with very nearly orthogonal in-plane basis vectors $[01\bar{1}]^*$ and $[013]^*$. In combination with the out-of-plane basis vector $[100]^*$, such a reciprocal space sublattice accounts for virtually all (certainly all strong) reflections observed in XRD powder patterns. Given that $[100]^*$ is not orthogonal to the

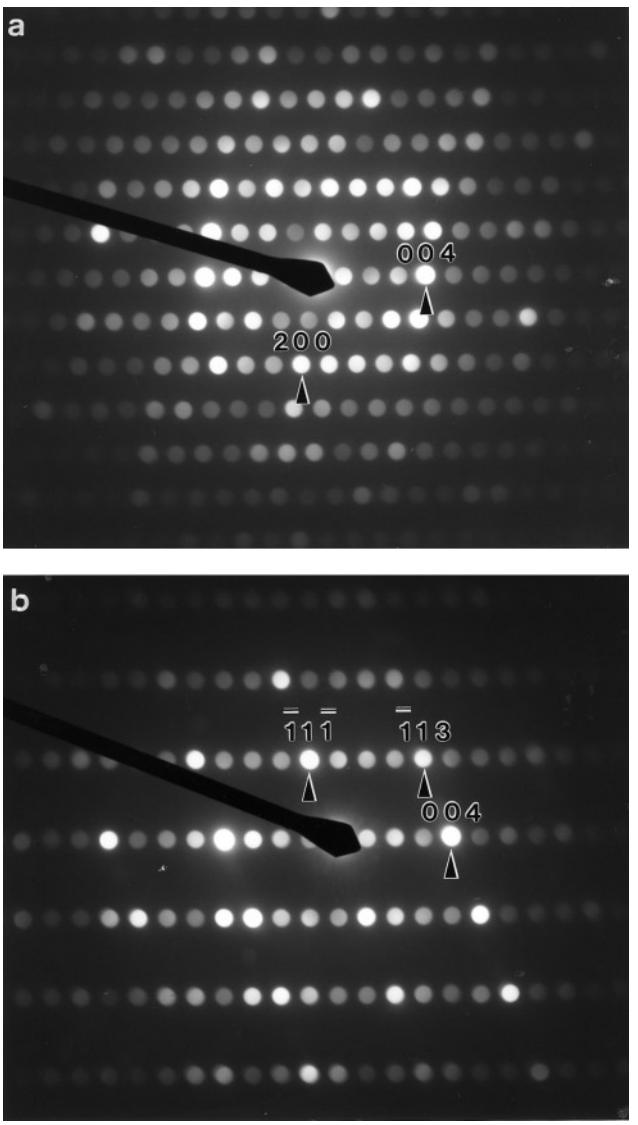

FIG. 6. (a) [010] and (b) [110] zone axis micro-diffraction patterns characteristic of the Series 2 phase.

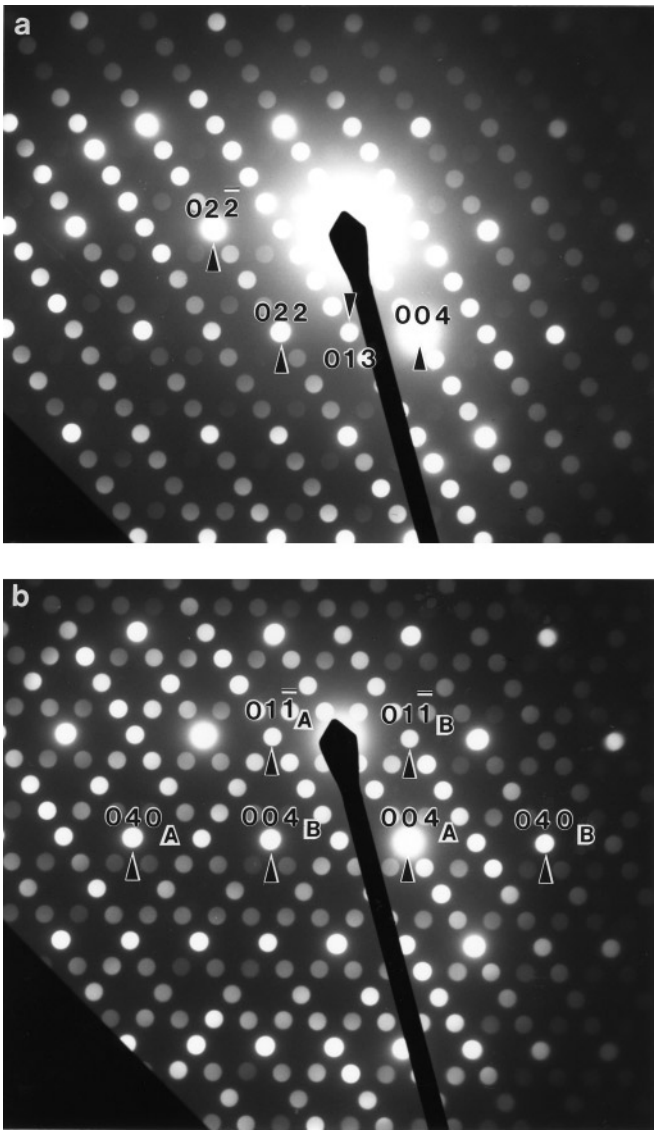

FIG. 7. (a) An essentially single twin variant micro-diffraction pattern of the Series 2 phase taken close to a [100] zone axis orientation. Very slight movement of the probe gave rise to the twinned [100] zone axis micro-diffraction pattern shown in (b). Such twinning was commonly observed and always occurs perpendicular to the $[01\bar{1}]^*$ direction of reciprocal space. Reflections belonging to the two (A and B) twin variants are labeled.

reciprocal space plane defined by $[01\bar{1}]^*$ and $[013]^*$, the exact reciprocal space twin relationship between the two twin variants requires a further EDP taken at a different orientation and from an area that also includes both twin variants—such as the [011] zone axis EDP shown in Fig. 8. The resultant reciprocal space twin relationship between the two twin variants is given by $[01\bar{1}]^*_A = -[01\bar{1}]^*_B$, $[013]^*_A = [013]^*_B$, and $[51\bar{1}]^*_A = [500]^*_B$, respectively.

Negas *et al.* (1) pointed out that "... the rapid reduction of $CeTaO_{4.5}$ (series 2) to $CeTaO_{4.17}$ (series 3) at 600°C.. suggests a transition between structurally similar materials ..." The crystallographic relationship between the Series 2 and 3 phases or between the Series 2 and the fully reduced $CeTaO_4$ phase, however, is not immediately apparent, at least not to the present authors! One reciprocal space relationship that is clearly significant is that all the various reduced and oxidized $CeTaO_{4+\delta}$ variants appear to have in common a parent pseudohexagonal reciprocal space plane (cf. the [100] zone axis EDP of the Series 3 phase shown in Fig. 9a with the [001] zone axis micro-diffraction pattern of the fully reduced $CeTaO_4$ phase shown in Fig. 9b. The approximately C-centered heavy metal atom array of the [001] zone axis projection of the crystal structure of the fully reduced $CeTaO_4$ phase shown in Fig. 1b is the real space analogue of the reciprocal space pseudohexagonal parent sublattice of reflections in Fig. 9b. In projection, it would therefore appear that such a C-centered heavy metal atom array must be in common for all oxidized and reduced $CeTaO_{4+\delta}$ phases.

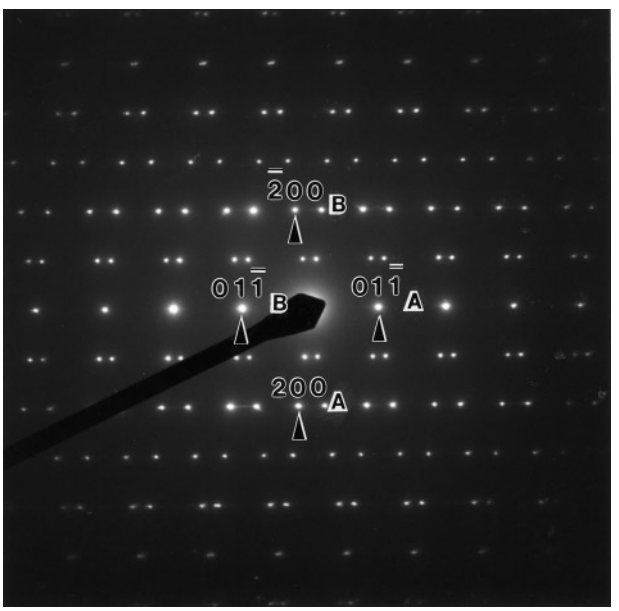

FIG. 8. Shows an [011] zone axis EDP of the Series 2 phase taken from an area including both twin variants. Reflections belonging to the two (A and B) twin variants are labeled.

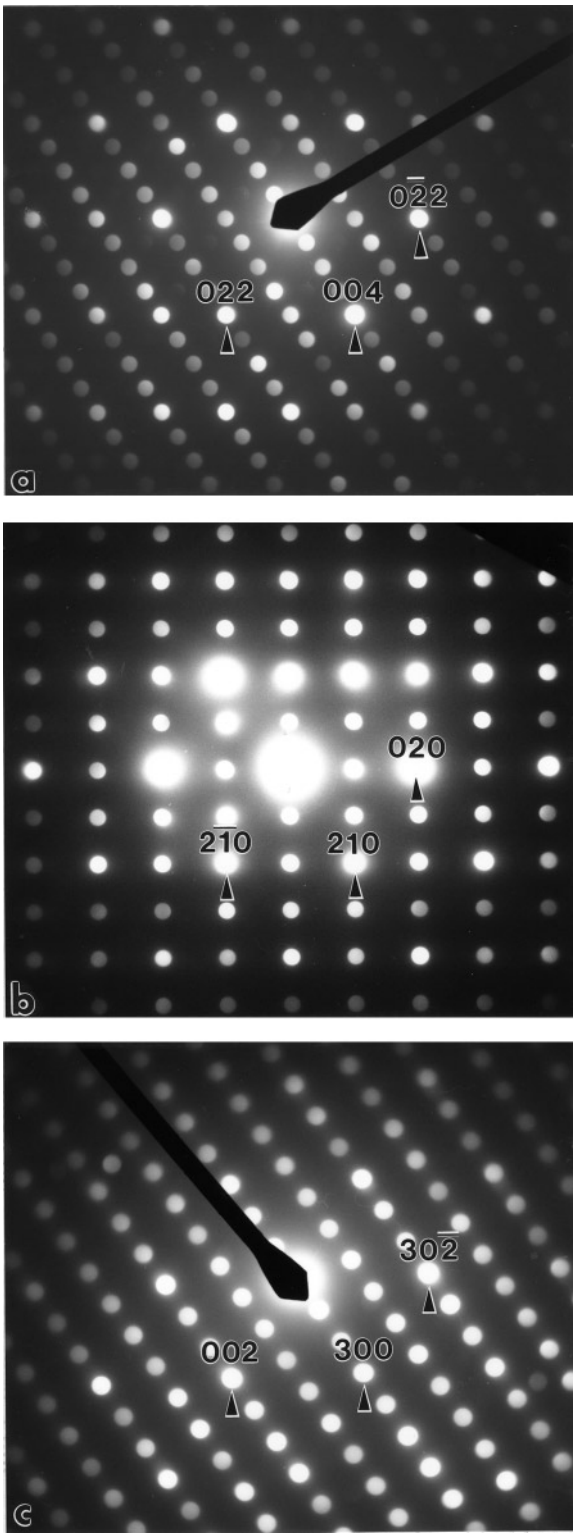

FIG. 9. Shows micro-diffraction patterns characteristic of (a) the Series 2 phase at a [100] zone axis orientation, (b) the fully reduced $CeTaO_4$ phase at an [001] zone axis orientation, and (c) the Series 4 phase at an [010] zone axis orientation. Note that all three phases have in common a parent pseudohexagonal reciprocal space sublattice (corresponding to the labeled reflections), at least in projection.

The Series 4 Phase

Roth *et al.* (2) reported an $a = 10.095$, $b = 3.821$, $c = 6.524$ Å, $\beta = 112.40^\circ$ monoclinic cell for the 950°C Series 4 phase. Our XRD results gave a very similar monoclinic subcell ($a = 10.107(4), b = 3.836(2), c = 6.542(3)$ Å, $\beta = 112.67(3)^\circ$). Electron diffraction, however, revealed the presence of weak additional $\mathbf{G} \pm \frac{1}{2}\mathbf{b}^*$ satellite reflections (see the [100] and [001] zone axis EDPs of Fig. 10) which require doubling of the b axis to 7.672 Å. These additional satellite reflections are, however, often quite streaked perpendicular to $\mathbf{b}^*$. The most likely space group symmetry is $P2/m$ or $P2_1/m$.

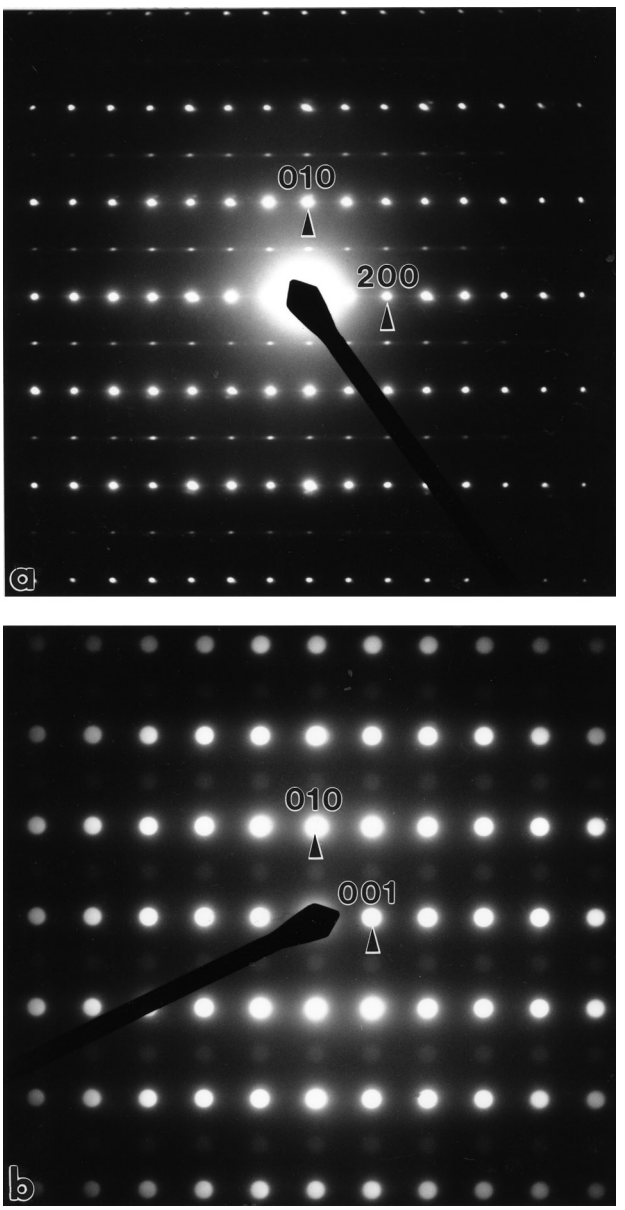

FIG. 10. Shows (a) [001] and (b) [100] zone axis EDPs characteristic of the Series 4 phase. Indexation is with respect to the strongly scattering $a \sim 10.1$, $b = 3.8$, $c = 6.5$ Å, $\beta \sim 112.7^\circ$ subcell. Note the presence of weak additional $\mathbf{G} \pm \frac{1}{2}\mathbf{b}^*$ type satellite reflections in both (a) and (b).

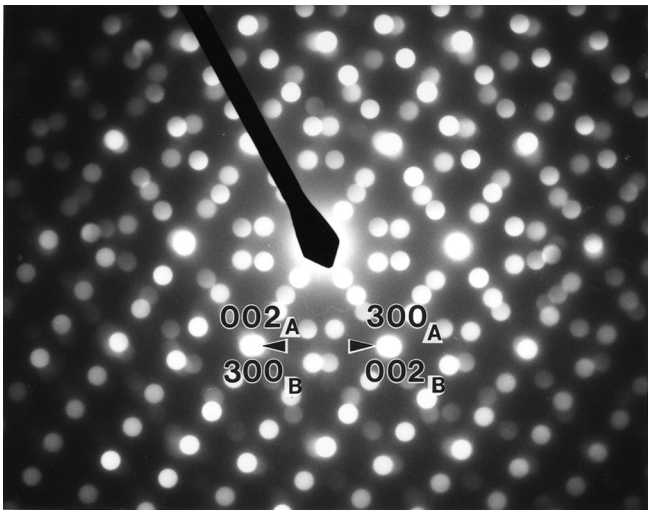

FIG. 11. A twinned [010] zone axis micro-diffraction pattern of the Series 4 phase taken from an area containing both twin variants. Note that the twinning again occurs perpendicular to the same reciprocal space direction with respect to the strong parent pseudohexagonal reciprocal space sublattices of Fig. 9—in this case corresponding to the $[30\bar{2}]^*$ direction of reciprocal space with respect to the reciprocal lattice of the Series 4 phase.

Twinning was again endemic. Figure 9c, for example, shows a single twin variant micro-diffraction pattern taken at the [010] zone axis orientation—the zone axis orientation for the Series 4 phase showing the parent pseudohexagonal reciprocal space sublattice common to the Series 2, 3, and 4 phases (cf. with Figs. 9a and 9b). The corresponding [010] micro-diffraction pattern from an area containing both twin variants is shown in Fig. 11. The twinning again occurs perpendicular to the same reciprocal space direction with respect to the strong parent pseudohexagonal reciprocal space sublattice—in this case corresponding to the $[30\bar{2}]^*$ direction of reciprocal space with respect to the reciprocal lattice of the Series 4 phase. The reciprocal space twin relationship between the two twin variants is thus given by $[300]^*_A = [002]^*_B$, $[002]^*_A = [300]^*_B$, and $[010]^*_A = -[010]^*_B$, respectively.

4. CONCLUSIONS

The low temperature and reversible nature of the phase transformations from stoichiometric $Ce^{+III}TaO_4$ to the oxidized Series 2 phase and from the Series 2 to the Series 3 phase at a somewhat higher temperature demand that there must be close structural relationships between all these phases, presumably relationships which involve minimal bond breaking and reconstruction. The higher temperatures required to obtain the Series 4 phase and the nonreversibility

of the phase transformation suggest that this phase is not necessarily so closely structurally related. While the structural relationship between stoichiometric $Ce^{+III}TaO_4$ and the Series 3 phase is, at least in principle, reasonably clear-cut ($CeTaO_{4.17}$ stoichiometry and a $3 \times \mathbf{b}$ superstructure of the 650°C Series 2 phase requires the insertion of an additional two extra oxygen atoms per supercell into the interstices of the parent, fully reduced structure plus a concurrent oxidation of 4 Ce^{+III} ions to Ce^{+IV} ions), the relationship between the Series 2 and Series 4 phases and $Ce^{+III}TaO_4$ is by no means so apparent.

ACKNOWLEDGMENTS

A-K. Larsson gratefully acknowledges financial support from STINT via the Swedish Natural Science Research Council (NFR). The authors acknowledge fruitful discussions with Drs. J. G. Thompson and N. Bliznyiuk and Professor A. D. Rae.

REFERENCES

1. T. Negas, R. S. Roth, C. L. McDaniel, H. S. Parker, and C. D. Olsen, *Mater. Res. Bull.* **12,** 1161–1171 (1977).
2. R. S. Roth, T. Negas, H. S. Parker, D. B. Minor, and C. Jones, *Mater. Res. Bull.* **12,** 1173–1182 (1977).
3. R. S. Roth, T. Negas, H. S. Parker, D. B. Minor, C. D. Olsen, and C. Skarda, *in* "The Rare Earths in Modern Science and Technology" (G. J. McCarthy and J. J. Rhyne, Eds.), pp. 163–171, (1978).
4. R. J. Cava, T. Negas, R. S. Roth, H. S. Parker, D. B. Minor, and C. D. Olsen, *in* "The Rare Earths in Modern Science and Technology" (G. J. McCarthy and J. J. Rhyne, Eds.), pp. 181–187 (1978).
5. T. A. Kurova and V. B. Aleksandrov, *Dokl. Akad. Nauk. SSSR* **201,** 1095–1098 (1971).
6. A. Santoro, M. Marezio, R. S. Roth, and D. Minor, *J. Solid State Chem.* **35,** 167–175 (1980).
7. R. J. Cava and R. S. Roth, *J. Solid State Chem.* **36,** 139–147 (1981).
8. B. G. Hyde and S. Andersson, "Inorganic Crystal Structures." Wiley, New York, 1989.